Draft version January 2, 2019
Typeset using LaTeX **twocolumn** style in AASTeX62

Asteroseismology of massive stars with the TESS mission: the runaway β Cep pulsator PHL 346 = HN Aqr

Gerald Handler,[1] Andrzej Pigulski,[2] Jadwiga Daszyńska-Daszkiewicz,[2] Andreas Irrgang,[3] David Kilkenny,[4] Zhao Guo,[5] Norbert Przybilla,[6] Filiz Kahraman Aliçavuş,[1] Thomas Kallinger,[7] Javier Pascual-Granado,[8] Ewa Niemczura,[2] Tomasz Różański,[2] Sowgata Chowdhury,[1] Derek L. Buzasi,[9] Giovanni M. Mirouh,[10] Sergio Simón-Díaz,[11,12] Ehsan Moravveji,[13] and Peter De Cat[14]

[1] *Nicolaus Copernicus Astronomical Center, Bartycka 18, 00-716 Warsaw, Poland*
[2] *Astronomical Institute Wrocław University, ul. Kopernika 11, 51-622 Wrocław, Poland*
[3] *Dr. Karl Remeis-Observatory & ECAP, Astronomical Institute, Friedrich-Alexander University Erlangen-Nürnberg (FAU) Sternwartstr. 7, 96049 Bamberg, Germany*
[4] *Department of Physics & Astronomy, University of the Western Cape, Private Bag X17, Bellville 7535, South Africa*
[5] *Center for Exoplanets & Habitable Worlds, Department of Astronomy & Astrophysics Eberly College of Science, The Pennsylvania State University, 525 Davey Lab, University Park, PA 16802, USA*
[6] *Institut für Astro- und Teilchenphysik, Universität Innsbruck, Technikerstr. 25/8, 6020 Innsbruck, Austria*
[7] *Institute for Astrophysics, University of Vienna, Türkenschanzstrasse 17, 1180 Vienna, Austria*
[8] *Instituto de Astrofísica de Andalucía (IAA-CSIC), Glorieta de Astronomía s\n, E-18008 Granada, Spain*
[9] *Dept. of Chemistry & Physics, Florida Gulf Coast University, 10501 FGCU Blvd. S., Fort Myers, FL 33965, USA*
[10] *Astrophysics Research Group, Faculty of Engineering and Physical Sciences, University of Surrey, Guildford GU2 7XH, UK*
[11] *Instituto de Astrofísica de Canarias, E-38200 La Laguna, Tenerife, Spain*
[12] *Departamento de Astrofísica, Universidad de La Laguna, E-38205 La Laguna, Tenerife, Spain*
[13] *Instituut voor Sterrenkunde, KU Leuven, Celestijnenlaan 200D, 3001 Leuven, Belgium*
[14] *Royal Observatory of Belgium, Ringlaan 3, B-1180 Brussel, Belgium*

(Received January 7, 2019; Revised January 1, 2019; Accepted January 2, 2019)

Submitted to ApJL

ABSTRACT

We report an analysis of the first known β Cephei pulsator observed by the TESS mission, the runaway star PHL 346 = HN Aqr. The star, previously known as a singly-periodic pulsator, has at least 44 oscillation modes excited, both in the g- and p-mode domains. Analysis of archival data implies that the amplitude and frequency of the dominant mode and the stellar radial velocity were variable over time. A binary nature can be speculated about, but would be inconsistent with the inferred ejection velocity from the Galactic disc of $420\,\mathrm{km\,s^{-1}}$, which is too large to be survived by a runaway binary system. A kinematic analysis of the star results in an age constraint (23 ± 1 Myr) to be imposed on asteroseismic modelling. Our attempts to match the excitation of the observed frequency spectrum resulted in pulsation models that were too young. Hence, asteroseismic studies of runaway pulsators can become vital in tracing the evolutionary history of such objects. TESS is now opening up massive stars for detailed asteroseismic investigation.

Keywords: stars: early-type — stars: individual (HN Aqr) — stars: interiors — stars: kinematics and dynamics — stars: massive — stars: oscillations (including pulsations)

1. INTRODUCTION

The Transiting Exoplanet Survey Satellite (TESS) is a NASA mission whose primary objective is to discover hundreds of transiting planets smaller than Neptune with host stars bright enough for spectroscopic follow-up to measure planetary masses and atmospheric compositions (Ricker et al. 2015). TESS was launched in April 2018 and has commenced its almost-all-sky survey of bright stars ($4 < I_c < 13$) in a wide red-bandpass filter. Strips of $24° \times 96°$ strips on the sky are observed

Corresponding author: Gerald Handler
gerald@camk.edu.pl

to deliver time series of between $27 - 351$ d length depending on ecliptic latitude. In the first two years of operation 200 000 pre-selected targets will be monitored with 2-min cadence, and full-frame images that enable precision photometry of about 30 million stars are obtained every 30 minutes.

The characterization of extrasolar planets requires information about their host stars. One of the methods that yields this information is asteroseismology (e.g., Lundqvist et al. 2018), the study of stellar interiors by utilizing their pulsations as seismic waves. Asteroseismology comes at no additional cost to planet-search photometric missions as the observational technique is essentially the same: high-accuracy time-resolved photometry. Consequently, asteroseismology and exoplanet space missions often are combined (e.g., Michel et al. 2006; Gilliland et al. 2010), just like TESS.

Because TESS will be the first precision photometry mission that surveys almost the whole sky, some types of stars that were not prime targets for searches for extrasolar planets will now be observed in large amounts. In particular, the asteroseismic potential of hot massive stars does not appear to have been fully exploited yet. Pedersen et al. (2019) give a first summary of what TESS can do for OB star astrophysics. In this Letter, we report a study of the first known β Cephei pulsator observed with the TESS mission, PHL 346 = HN Aqr.

1.1. *PHL 346 = HN Aqr*

PHL 346 is a star of $V = 11.44$ located at a Galactic latitude of $b \approx 58^o$. Kilkenny et al. (1977) classified it with spectral type B1, and Keenan et al. (1986) reported a surface gravity consistent with an evolved main-sequence evolutionary status and Pop. I metal abundances. Given the radial velocity they measured ($+66 \pm 10\,\mathrm{km\,s^{-1}}$), Keenan et al. (1986) had to conclude that PHL 346 would not have had enough time to attain such a high Galactic latitude within its lifetime and thus needed to have been formed far from the Galactic plane. This puzzling result was amended by Ramspeck et al. (2001) who, based on a new spectroscopic analysis and the first proper motion measurement of PHL 346, reconciled the stellar flight time with its lifetime, meaning the star could have been formed in and ejected from the Galactic plane.

PHL 346 was also the subject of several studies that resulted in determinations of its effective temperature and surface gravity. These comprised optical spectroscopy (Kilkenny & Lydon 1986; Keenan et al. 1986; Ryans et al. 1996; Ramspeck et al. 2001), ultraviolet spectroscopy (Niemczura & Daszyńska-Daszkiewicz 2005), Strömgren photometry (Kilkenny et al. 1977; Handler 2011) as well as Geneva and Walraven photometry (Heynderickx et al. 1994). Summarizing these results and using bolometric corrections from Flower (1996) suggests that a range of basic parameters $T_{\rm eff} = 22200 \pm 1500$ K, $\log g = 3.7 \pm 0.2$, $M_{\rm bol} = -5.2 \pm 0.3$ and $[M/H] = 0.2 \pm 0.1$, should contain the parameter space in which a seismic model for HN Aqr ought to be located. Furthermore, the literature results also imply a macroturbulence $\zeta = 14 \pm 6\,\mathrm{km\,s^{-1}}$, projected rotational velocity $v \sin i = 45\,\mathrm{km\,s^{-1}}$, $[M/H] = 0.21$, and $E(B-V) = 0.055 \pm 0.020$. The Gaia DR2 parallax $\pi = 0.10 \pm 0.08$ mas for HN Aqr (Gaia Collaboration et al. 2016, 2018; Luri et al. 2018) cannot be used to constrain the stellar luminosity better, but it is consistent with the results above.

β Cephei-type pulsations of PHL 346 were discovered by Waelkens & Rufener (1988) and confirmed by Kilkenny & van Wyk (1990). The star was also observed during the ASAS survey (Pigulski & Pojmański 2008) and by Handler & Shobbrook (2008). All these authors detected the same single oscillation frequency near $6.566\,\mathrm{d^{-1}}$. Heynderickx et al. (1994) and Cugier et al. (1994) suggested this pulsation is due to a nonradial $l = 1$ mode. On the other hand, Handler & Shobbrook (2008) derived $l = 2$ or 4 for this oscillation, but noted a possible problem with the U filter data their identification critically hinged upon.

2. OBSERVATIONS

PHL 346 was observed with the TESS mission in Sector 2, from August 23, 2018 to September 20, 2018 with 2-min integrations. 18317 brightness measurements were secured over a time base of $\Delta T = 27.4$ d, with a duty cycle of 92.8%. The photometry was downloaded from MAST[1], and the PDC_SAP fluxes were converted into magnitude. No further manipulations with the data were made. The second part of the light curve is shown in Fig. 1. Clearly, HN Aqr is not a singly-periodic variable. Variations in the mean light level as well as changes in the amplitude of the dominant short-period signal are visible.

3. ANALYSIS

3.1. *Periodicities in the TESS light curve*

We analyzed the data using five methods and discuss these approaches in some detail in view of analyses of future TESS data sets. Perhaps the most widely used and classical method is single-frequency power spectrum analysis and simultaneous multi-frequency sine-wave fit-

[1] https://mast.stsci.edu/portal/Mashup/Clients/Mast/Portal.html

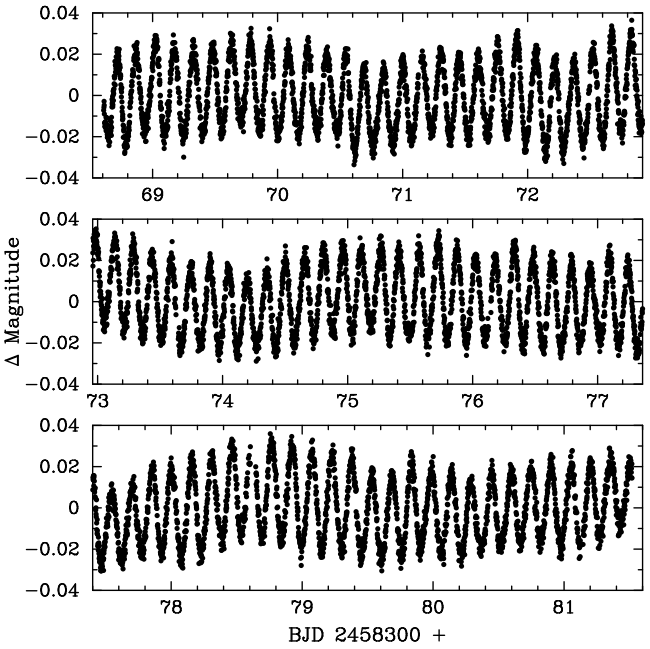

Figure 1. Light curve from 13 days of TESS observations of HN Aqr.

ting with input parameter optimization, such as employed in the Period04 (Lenz & Breger 2005) package. The sine-wave fits are subtracted from the data and the residuals examined for the presence of further periodicities.

Using this procedure repeatedly, one needs to subtract 90 frequencies from the data to reach the level of the noise (tallest noise peaks around 0.15 mmag). Seventy-one of these frequencies would be statistically significant according to the $S/N > 4$ criterion by Breger et al. (1993), comprising 31 signals between 0.13 and 2.68 d^{-1}, 38 signals between 5.38 and 12.24 d^{-1}, and two combination frequencies. Eight of these signals have neighbors closer than the Rayleigh frequency resolution of the 27.4-d data set would allow to detect.

Secondly we again used the classical approach, but modeled the background noise in the Fourier spectrum in log-log space with the equation:

$$a(\nu) = \frac{a_0}{1 + (\frac{\nu}{\nu_0})^{\lambda}} + P_0, \qquad (1)$$

where P_0 is a constant Gaussian noise term, a and ν_0 are the amplitude and characteristic frequency describing the red noise, respectively.

We again used the $S/N > 4$ criterion to assess the significance of detection. Additionally, we compared the extracted and optimized frequencies with the local original Fourier amplitudes, and only accepted the signals comparable in amplitude, to prevent spurious peaks generated by the pre-whitening process (Van Reeth et al. 2015). In that way, 44 frequencies were obtained, including 14 between 0.28 to 1.49 d^{-1}, 29 between 5.45 and 12.25 d^{-1}, and one harmonic. Five of these 44 frequencies have neighboring signals within 69 and 99% of the Rayleigh frequency resolution.

Method three used the MIARMA gap-filling method (Pascual-Granado et al. 2015) to improve the spectral window function of the data, particularly in view of the 1.45-d gap in the middle of the time series due to data download. This modified light curve was frequency analyzed with the SigSpec algorithm (Reegen 2007), resulting in a total of 114 detected signals (43 between 0.13 and 4.19 d^{-1}, 66 between 5.27 and 12.27 d^{-1}, and five combination frequencies), 15 of which had neighbors within the Rayleigh frequency resolution.

The fourth technique employed a Bayesian algorithm (Kallinger & Weiss 2016) allowing a probabilistic assessment of the significance of signal detection. It was run twice, once allowing only a single frequency to represent a peak in the amplitude spectrum (equivalent to multi-frequency sine-wave fitting), and the other time allowing close frequency doublets (spacing $\leq 3/\Delta T = 0.11\,\mathrm{d}^{-1}$) which is known to yield excellent results in case of unresolved frequency multiplets (Kallinger et al. 2017). With the single-frequency fitting approach, 41 signals were detected, including 23 between 0.13 to 1.88 d^{-1}, 17 between 5.46 and 11.27 d^{-1}, and one harmonic. Seven of these 41 frequencies had neighboring signals between 63 and 91% of the Rayleigh frequency resolution. With the alternative approach, 70 frequencies were retrieved, 33 of them between 0.06 and 2.687 d^{-1}, 36 between 5.46 and 11.37 d^{-1}, and one harmonic. Interestingly, the algorithm identified the dominant pulsation frequency as a close doublet of $6.555 \pm 0.003\,\mathrm{d}^{-1}$ (2.9 mmag amplitude) and $6.5666 \pm 0.0005\,\mathrm{d}^{-1}$ (18.1 mmag amplitude).

The fifth method used was a Morley wavelet transform (Torrence & Compo 1998). Output from this approach reflected the amplitude modulation of the short-period pulsations (Fig. 1). Of particular interest is the low-frequency region ($f < 2\,\mathrm{d}^{-1}$), where considerable changes in the amplitudes of individual signals are visible, however in most cases with some degree of regularity indicating multifrequency beating.

To reconcile the outcome of the different methods we have compared the results of the first four techniques. From the Bayesian approach we selected the outcome of the method allowing close doublets that essentially comprises that of the single-frequency trial as a subset. The four methods yielded fairly consistent results for strong, well-resolved signals, but diverged in frequency regions where densely spaced signals were present.

To provide a set of pulsation frequencies that can be reasonably safely used for asteroseismic investigations, we only accepted signals detected by at least three of the methods independently. The amplitudes of these signals had to exceed the noise level $a(\nu)$ (Eq. 1) by factors of 4 (independent signals) and 3.5 (combination frequencies), respectively. The resulting list of frequencies is given in Table 1. Most of the frequency values were adopted from the Bayesian method, with the exception of two undetected signals that were taken from the multifrequency fit. Error estimates come from the Bayesian method, which correspond well to the least-squares errors for well-separated signals, taking systematic uncertainties of closely-spaced frequencies into account. As it is not well known how much data processing affects the low-frequency domain, the longest-period signals reported here should be treated with caution. Some steps of prewhitening of the TESS data are illustrated in Fig. 2. Our multifrequency fit leaves a residual scatter of 3.2 mmag per point (590 ppm/hr) containing residual stellar variability contributing some 10% to the total scatter.

Table 1. Multifrequency solution for our TESS photometry of HN Aqr. Error estimates for the independent frequencies are given in braces in units of the last significant digit; the errors on the amplitudes are about ±0.03 mmag.

ID	Freq. (d^{-1})	Ampl. (mmag)	S/N
f_1	0.2241(8)	0.93	5.1
f_2	0.2731(7)	0.88	5.0
f_3	0.3421(2)	4.00	24.2
f_4	0.3881(5)	1.55	9.7
f_5	0.4522(10)	0.84	5.5
f_6	0.4844(17)	0.75	5.0
f_7	0.5260(4)	2.06	14.0
f_8	0.6058(4)	1.67	11.8
f_9 [a]	0.697(1)	1.09	8.0
f_{10}	1.0401(10)	0.54	4.5
f_{11}	1.1461(7)	0.89	7.7
f_{12} [b]	1.259(1)	0.59	5.3
f_{13}	1.3589(6)	1.12	10.3
f_{14}	1.4919(7)	0.87	8.2
f_{15}	1.8873(10)	0.45	4.6
f_{16}	1.9134(27)	0.39	4.0
f_{17}	5.4562(8)	0.79	12.4
f_{18}	5.543(3)	0.27	4.2
f_{19}	5.684(2)	0.25	4.0
f_{20}	6.079(1)	0.39	6.4
f_{21}	6.245(2)	0.83	13.8
f_{22}	6.267(1)	1.06	17.6
f_{23}	6.371(2)	0.38	6.4
f_{24} [c]	6.5653(5)	20.65	349.4
f_{25}	7.747(1)	0.60	10.9
f_{26}	7.903(1)	0.58	10.7
f_{27}	8.083(1)	0.69	12.7
f_{28}	8.273(3)	0.29	5.4
f_{29}	8.649(1)	0.64	12.1
f_{30}	8.829(1)	0.54	10.5
f_{31}	9.021(2)	0.26	5.0
f_{32}	9.194(1)	0.61	11.9
f_{33}	9.486(2)	0.45	8.9
f_{34}	9.567(5)	0.23	4.5
f_{35}	9.677(2)	0.38	7.6
f_{36}	9.714(2)	0.36	7.3
f_{37}	9.801(3)	0.26	5.2
f_{38}	9.902(3)	0.30	6.0
f_{39}	10.043(2)	0.37	7.6
f_{40}	10.095(3)	0.29	6.0
f_{41}	10.226(2)	0.34	7.0
f_{42}	10.380(2)	0.44	9.0
f_{43}	10.455(3)	0.22	4.6
f_{44}	11.267(2)	0.37	8.0
$2f_{21}$	11.367(3)	0.22	4.7
$f_{21} + f_{26}$	12.249(2)	0.23	5.1
$2f_{26}$	13.1306(7)	1.13	26.1
$f_{26} + f_{27}$	14.312(1)	0.19	4.5
$f_{26} + f_{28}$	14.468(1)	0.15	3.6
$f_{26} + f_{29}$	14.649(1)	0.18	4.3

[a] Likely a close doublet (frequencies 0.679 and 0.715 d^{-1}).

[b] Likely a close doublet (frequencies 1.241 and 1.269 d^{-1}).

[c] Possibly a close doublet; see main text.

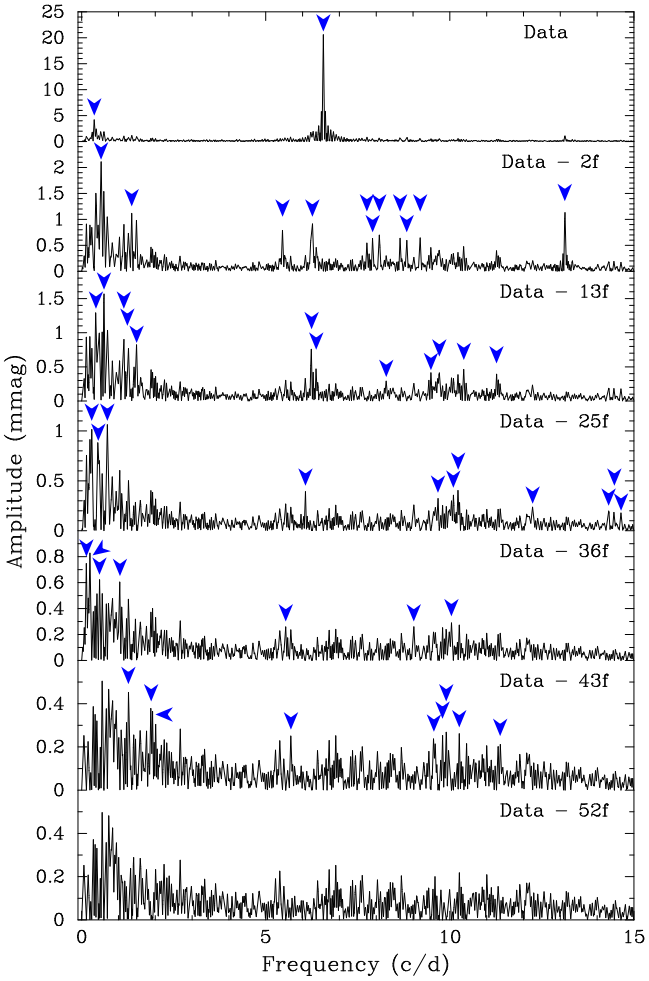

Figure 2. Fourier spectra of the TESS observations of HN Aqr. The blue arrows denote frequencies that are prewhitened in the panel below and correspond to the 50 signals listed in Table 1.

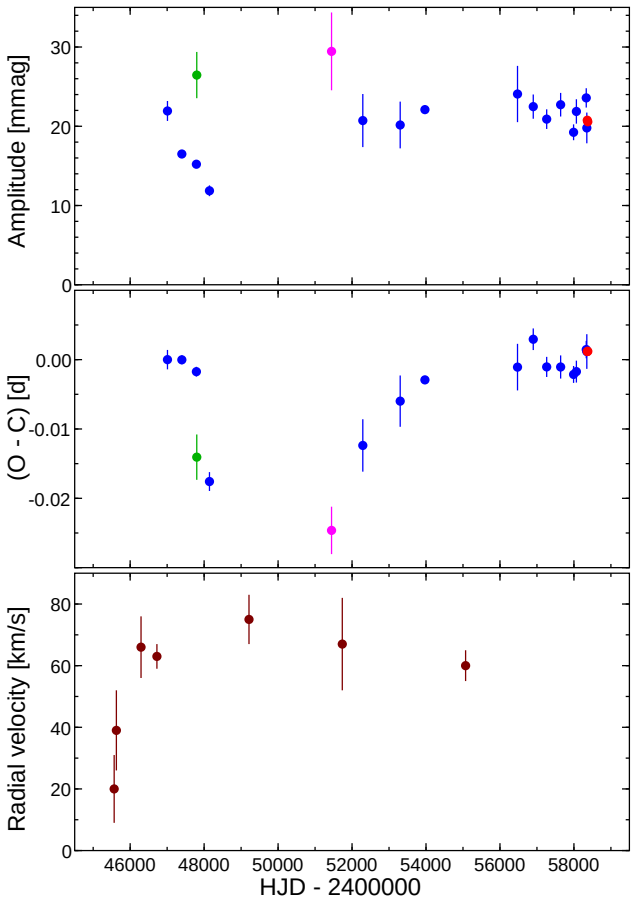

Figure 3. Top: Amplitude of the dominant mode in HN Aqr. The values derived from IUE, NSVS, and TESS photometry are shown with green, pink, and red dots, respectively, the remaining ones with blue dots. Middle: The O − C diagram for the times of maximum light of this mode calculated using the ephemeris: $T_{\max} = 2447008.89183 + 0.15231625 \times E$, where E is the number of pulsation cycles elapsed since the initial epoch. Bottom: Radial velocities of HN Aqr.

The low-frequency domain of detected signals extends up to $1.92\,\mathrm{d}^{-1}$. The large number of frequencies implies a pulsational origin. There is no evidence of a rotational or binary-induced modulation, or of a regular period spacing. A re-occurring frequency spacing is present within the signals in the p-mode domain ($\Delta f \approx 0.183\,\mathrm{d}^{-1}$), which may be due to rotational splitting. No multiplets were identified with confidence; the best candidate consists of frequencies $f_{27} - f_{30}$ which could be part of an $l = 2$ quintuplet with the $m = 0$ mode missing.

3.2. *Stability of the period and amplitude*

Thirty years have passed since pulsation in PHL 346 was discovered. Thus the long-term stability of the period and amplitude of the dominant pulsation mode can be studied. We gathered all available time-series photometry of the star (Waelkens & Rufener 1988; Kilkenny & van Wyk 1990; Handler & Shobbrook 2008; Pigulski & Pojmański 2008). Additionally, we include some previously unpublished observations from 1989 and 1990 by one of us (DK), as well as NSVS (Woźniak et al. 2004), and ASAS-SN (Shappee et al. 2014) data.

The resulting O − C diagram and amplitudes over time are shown in Fig. 3. The amplitude of the dominant mode remained relatively stable over 30 years at a level of about 22 mmag and dropped only in the late 1980s and early 1990s, down to 11.9 ± 0.7 mmag in 1990. (Expectedly the amplitude in the UV was higher than in the visual.) During this drop, the O − C diagram shows a significant period change: the 1990 value of O − C is ≈ 25 minutes off the ephemeris. We checked

whether the shape of the O−C diagram can be explained in terms of the light-time effect in a binary system, with no satisfactory solution. In any case, such an orbit needs to be highly eccentric ($e \gtrsim 0.7$) with periastron passage in the mid 1990's, when unfortunately a gap of almost a decade in the photometric data occurs. This would be also the time when large radial-velocity (RV) changes would occur. We therefore gathered all available radial-velocity data for HN Aqr (Keenan et al. 1986; Kilkenny & Muller 1989; Hambly et al. 1996; Ramspeck et al. 2001; Lynn et al. 2002), and plot them in the lower panel of Fig. 3). Although there is no large change of RV at the predicted time of the periastron passage, the first two RVs (Kilkenny & Muller 1989), are significantly different. Thus there is some inconsistency between the O−C diagram and the RV data, which may indicate that motion in a binary is not the main reason for period changes in HN Aqr.

Summarizing, in view of the large uncertainties of RVs, the presence of pulsations that increase the scatter of RVs and the large gap in photometric data which causes cycle count ambiguities in the 1990s, the results as to the binarity of the star are inconclusive.

3.3. *Spectroscopy and kinematics*

High-resolution ($R \approx 35\,000$) spectra of HN Aqr were taken with the UVES spectrograph (Dekker et al. 2000) attached to the VLT-UT2 at the European Southern Observatory (ESO) on the night of August 27, 2009. Integration times of 1150 s at both the blue and the red arm led to S/N ratios of about 150 − 190 in the range of 304 − 669 nm, and around 70 up to 1043 nm.

Using the analysis strategy described by Irrgang et al. (2014), we derive $T_{\rm eff} = 22290 \pm 450$ K, $\log g = 3.84 \pm 0.10$, $v \sin i = 30.3 \pm 0.3\,{\rm km\,s^{-1}}$, a macroturbulence $\zeta = 18 \pm 2\,{\rm km\,s^{-1}}$, a microturbulence $\xi = 8 \pm 1\,{\rm km\,s^{-1}}$, and differential abundances that are about 0.3 dex larger than that of reference stars in the solar neighborhood (Nieva & Przybilla 2012). The radial velocity at the time of measurement was $60 \pm 5\,{\rm km\,s^{-1}}$ (heliocentrically). Utilizing non-LTE model atmospheres and spectra calculated with the TLUSTY and SYNSPEC codes (Hubeny & Lanz 2017) alternatively, we determined $T_{\rm eff} = 22400 \pm 300$ K, $\log g = 3.80 \pm 0.06$, $v \sin i = 26 \pm 4\,{\rm km\,s^{-1}}$, $\zeta = 20 \pm 7\,{\rm km\,s^{-1}}$, $\xi = 14 \pm 1\,{\rm km\,s^{-1}}$, and abundances of $C = 8.78 \pm 0.07$, $N = 8.20 \pm 0.05$, $O = 8.90 \pm 0.08$, $Si = 7.76 \pm 0.07$, and $Fe = 7.66 \pm 0.07$. These values agree well with each other and the literature results, but imply a somewhat less evolved status of the star.

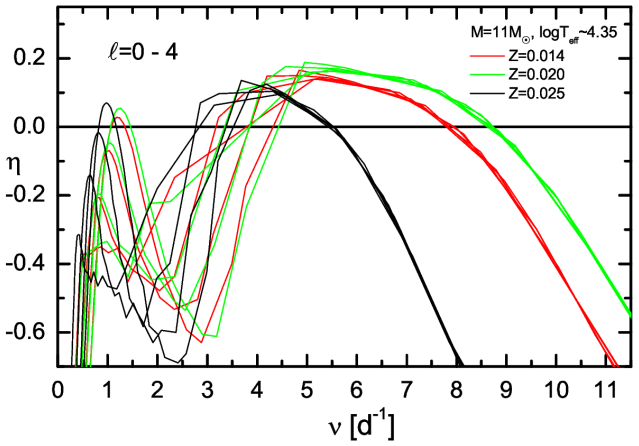

Figure 4. Effect of metallicity on pulsational driving of modes with $0 \le l \le 4, m = 0$ for a 11 $M_\odot$ model of HN Aqr. Modes with a stability parameter $\eta > 0$ are driven. An initial hydrogen abundance $X = 0.71$ (Nieva & Przybilla 2012), OPAL opacities, the Asplund et al. (2009) element mixture and no convective core overshooting were used.

The increased metallicity agrees very well with a kinematic investigation based on the radial velocity, Gaia DR2 proper motions, and a derived spectrophotometric distance of 6.7±0.8 kpc (99% confidence interval; assuming a mass of $9.5 \pm 0.4\,M_\odot$). It suggests that the star stems from the inner part of the Galaxy (Galactocentric radius at disk intersection 2.3±0.4 kpc (68% confidence interval)). After taking the Galactic abundance gradients into consideration, the abundance pattern appears to be perfectly normal except for an underabundance of ~ 0.3 dex in carbon. there trajectories (for details, see Irrgang et al. 2013), we infer a flight time to the Galactic disk of 23 ± 1 Myr (68% confidence interval).

3.4. *Pulsational modeling*

We follow the methods by Daszyńska-Daszkiewicz et al. (2017) to model the pulsation spectrum of HN Aqr preliminarily, using the basic stellar parameters determined earlier. We attempt to match the observed pulsational instability domains (Sect. 3.1) and the age constraint of 23 ± 1 Myr from the kinematic analysis. The most important influence on mode stability is provided by the overall metallicity, as shown in Fig. 4.

However, solely increasing Z is not sufficient to reproduce the observed instability domains, in particular in the g-mode region. Increasing Z even further results in a more massive model that evolves too rapidly: the model with $Z = 0.025$ has an age of 13.5 Myr and a main sequence lifetime of 18.0 Myr. Possible ways out of this problem would be the inclusion of convective core overshooting prolonging the main sequence lifetime (a 11 $M_\odot$, $Z = 0.025$, $\alpha_{ov} = 0.2$, $\log T_{\rm eff} = 4.35$ model

has an age of 15.5 Myr), increasing the He abundance leading to models of lower mass, and modifications of the input opacities, in particular near $\log T = 5.46$, corresponding to an enhancement of the nickel opacity (see, e.g. Daszyńska-Daszkiewicz et al. 2017). Rotational splitting of nonradial modes is most likely not an option due to the low projected rotational velocity of the star.

4. SUMMARY AND CONCLUSIONS

TESS photometry of the pulsating runaway star HN Aqr provided the detection of 50 frequencies of variability with evidence for more. The star has rich p- and g-mode pulsation spectra. Some of the oscillation frequencies are formally unresolved during the 27.4-d time base of the observations, a problem expected to affect the analysis of other β Cephei and related types of pulsating stars as well. Hence we applied five different frequency analysis techniques whose combination resulted in a reliable solution.

The signals in the low-frequency domain are dominated by g-mode pulsation. The frequency spectrum is denser at the low-frequency end, which is expected for opacity-driven g modes, but the occurrence of internal gravity waves (e.g., Aerts & Rogers 2015) may also be suspected. The p-mode frequency region is surprisingly wide and spans some five radial overtones. We detected 28 frequencies in this domain, which could be explained by modes of $l \leq 2$ and their rotationally split components only. However, no clear evidence for such rotational splitting was detected, suggesting that modes of higher l are also present.

An analysis of archival data showed that the frequency and amplitude of the dominant mode, as well as the radial velocity of the star were not stable over the last 30 years. One may speculate about the presence of a binary companion, but this would be rather surprising because such systems should not survive the ejection of the star from the Galactic disc (Perets & Šubr 2012), and capture of a companion by a fast-moving runaway star is unfeasible. Furthermore, our Bayesian frequency analysis provided evidence that the dominant pulsation frequency of HN Aqr may be a close doublet, which would provide an alternative interpretation for its amplitude and frequency variations. Therefore, the star should be included in a long-term spectroscopic and photometric observing program.

Pulsational modeling shows that the observed pulsation spectrum cannot be reproduced by increasing the metallicity only; an increase in the opacities in certain stellar interior regions is required. Interestingly, the nature of HN Aqr as a runaway star provides additional constraints on the modeling, as the age of the models must be reconciled with the stellar flight time (23 ± 1 Myr). Our initial attempts in this direction were unsuccessful as we could not obtain models older than 18 Myr that would give a reasonable match to the observed pulsation spectrum. Asteroseismic studies of runaway pulsators with precise age determinations may become as important as the studies of pulsators in double-lined eclipsing binaries and can become vital in tracing the evolutionary history of such objects. HN Aqr may not be the only star that can be studied that way (e.g., see Table 1 of Perets 2009).

The analysis of the first β Cephei pulsator observed with TESS already demonstrates its potential for massive star asteroseismology. HN Aqr, over the last 30 years believed to pulsate in a single frequency, exhibits at least 44 independent modes. This is the level of progress that space photometry of lower-mass stars has already undergone thanks to the Kepler mission; TESS is now opening the domain of massive stars for in-depth asteroseismology as well.

Based on observations collected at the European Southern Observatory under ESO programme 383.D-0909(A).

Funding through NCN grant 2015/18/A/ST9/00578 is gratefully acknowledged. JDD acknowledges support from the NCN grant 2015/17/B/ST9/02082. GMM acknowledges funding by the STFC consolidated grant ST/R000603/1. GH thanks Daniel Heyndericxk for supplying the photometry by Waelkens & Rufener (1988) and David Jones for help in retrieving some archival data.

Facilities: TESS, ESO VLT-UT2, UVES, SAAO

Software: Period04 (Lenz & Breger 2005), SigSpec (Reegen 2007), MIARMA (Pascual-Granado et al. 2015)

REFERENCES

Aerts, C., Rogers, T., M., 2015, ApJ, 806, L33

J., Allende Prieto, C., & Kiselman, D., 2004, A&A, 417, 751

Asplund, M., Grevesse, N., Sauval, A. J., Scott, P., 2009, ARA&A, 47, 481
Breger, M., Stich, J., Garrido R. et al., 1993, A&A 271, 482
Cugier, H., Dziembowski, W. A., & Pamyatnykh, A. A. 1994, A&A, 291, 143
Daszyńska-Daszkiewicz, J., Pamyatnykh, A. A., Walczak, P. et al., 2017, MNRAS, 466, 2284
Dekker, H., D'Odorico, S., Kaufer, A., Delabre, B., & Kotzlowski, H. 2000, in Proc. SPIE, Vol. 4008, Optical and IR Telescope Instrumentation and Detectors, ed. M. Iye & A. F. Moorwood, 534
Dufton, P. L., Keenan, F. P., Kilkenny, D., et al., 1998, MNRAS, 297, 565
Flower, P. J. 1996, ApJ, 469, 355
Gaia Collaboration, Prusti, T., de Bruijne, J. H. J. et al., 2016, A&A, 595, A1
Gaia Collaboration, Brown, A. G. A., Vallenari, A. et al., 2018, A&A, 616, A1
Gilliland, R. L., Brown, T. M., Christensen-Dalsgaard, J. et al., 2010, PASP, 122, 131
Hambly, N. C., Wood, K. D., Keenan, F. P., et al., 1996, A&A, 306, 119
Handler, G., & Shobbrook, R. R., 2008, CoAst 156, 13
Handler, G., 2011, A&A, 528, A148
Heynderickx, D., Waelkens, C., & Smeyers, P. 1994, A&AS, 105, 447
Hubeny, I., & Lanz, T., 2017, arXiv:1706.01859
Irrgang, A., Wilcox, B., Tucker, E., Schiefelbein, L., 2013, A&A, 549, A137
Irrgang, A., Przybilla, N., Heber, U., et al. 2014, A&A, 565, A63
Kallinger, T., & Weiss, W. W., 2016, Proceedings of the Polish Astronomical Society volume 5, Second BRITE-Constellation Science Conference: Small satellites-big science, ed. K. Zwintz & E. Poretti (Polish Astronomical Society), 113
Kallinger, T., Weiss, W. W., Beck, P. G., et al., 2017, A&A, 603, A13
Keenan, F. P., Lennon, D. J., Brown, P. J. F. & Dufton, P. L., 1986, ApJ, 307, 694
Kilkenny, D., Hill, P. W., & Brown, A., 1977, MNRAS, 178, 123
Kilkenny, D. & Lydon, J. 1986, MNRAS, 218, 279
Kilkenny, D. & Muller, S., 1989, SAAO Circ. 13, 69
Kilkenny, D. & van Wyk, F. 1990, MNRAS, 244, 727
Lenz, P., & Breger, M., 2005, Comm. Asteroseism. 146, 53
Lundkvist, M. S., Huber, D., Silva Aguirre, V., & Chaplin, W. J., 2018, Handbook of Exoplanets, ed. Deeg H., Belmonte J., Springer International Publishing AG, id. 177
Luri, X., Brown, A. G. A., Sarro, L. M. et al., 2018, A&A, 616, A9
Lynn, B. B., Dufton, P. L., Keenan, F. P. et al., 2002, MNRAS, 336, 1287
Michel, E., Baglin, A., Auvergne, M., et al., 2006, ESA SP-1306, The CoRoT Mission Pre-Launch Status – Stellar Seismology and Planet Finding, ed. M. Fridlund, A. Baglin, J. Lochard & L. Conroy (Noordwijk: ESA Communication Production Office), 39
Montgomery, M. H., & O'Donoghue, D., 1999, Delta Scuti Star Newsletter, 13, 28
Napiwotzki, R., Schönberner, D., & Wenske, V. 1993, A&A, 268, 653
Niemczura, E., & Daszyńska-Daszkiewicz, J., 2005, A&A 433, 659
Nieva M.-F., & Przybilla N., 2012, A&A, 539, A143
North, P., & Nicolet, B., 1990, A&A 228, 78
Pascual-Granado, J., Garrido, R., & Suárez, J.-C., 2015, A&A, 575, A78
Pedersen, M. G., Chowdhury, S., Johnstone, C., et al., 2018, ApJL, submitted
Perets, H. B., 2009, ApJ, 698, 1330
Perets, H. B., Šubr, L., 2012, ApJ, 751, 133
Pigulski, A., & Pojmański, G., 2008, A&A, 477, 917
Ramspeck, M., Heber, U., & Moehler, S. 2001, A&A, 378, 907
Reegen, P., 2007, A&A, 467, 1353
Ricker, G. R., Winn, J. N.; Vanderspek, R. et al., 2015, Journal of Astronomical Telescopes, Instruments, and Systems, 014003
Ryans, R. S. I., Hambly, N. C., Dufton, P. L., & Keenan, F. P., 1996, MNRAS, 278, 132
Shappee, B. J., Prieto, J. L., Grupe, D., et al., 2014, ApJ, 788, 48
Torrence, C. & Compo, G. P., 1998, Bull. Amer. Meteor. Soc., 79, 61
Van Reeth, T., Tkachenko, A., Aerts, C., et al. 2015, A&A, 574, A17
Waelkens, C., & Rufener, F., 1988, A&A, 201, L5
Woźniak, P. R., Vestrand, W. T., Akerlof, C. W. et al. 2004, AJ, 127, 2436

APPENDIX

A. ADDITIONAL TABLES

This is for the information of TASC and the co-authors and will be removed in the version submitted to the journal.

Table 2. Determinations of basic parameters of PHL 346 from the literature.

$T_{\rm eff}$ (K)	log g	Ref.	Method
(5)	(6)	(7)	(8)
22000 ± 900	3.4 ± 0.2 [a]	Kilkenny et al. (1977)	Strömgren photometry
21000 ± 1500	3.6 ± 0.3 [b]	Kilkenny & Lydon (1986)	Optical spectroscopy
22600 ± 1000	3.6 ± 0.2 [c]	Keenan et al. (1986)	Optical spectroscopy
22900	3.882 [d]	Heynderickx et al. (1994)	Walraven photometry
22600	3.890 [e]	Heynderickx et al. (1994)	Geneva photometry
22300 ± 1000	3.7 ± 0.2 [f]	Ryans et al. (1996)	Optical spectroscopy
20700 ± 1000	3.58 ± 0.10 [g]	Ramspeck et al. (2001)	Optical spectroscopy
21500 ± 900	4.1 [h]	Niemczura & Daszyńska-Daszkiewicz (2005)	UV spectroscopy
23800 ± 900	3.6 ± 0.2 [j]	Handler (2011)	Strömgren photometry

[a] $M_v = -3.3 \pm 0.4$, $E(b-y) = 0.037$, calibration by Napiwotzki et al. (1993), H_β from Handler (2011)

[b] $v \sin i = 75 \pm 25\,\mathrm{km\,s^{-1}}$, $E(b-y) = 0.030$

[c] Macroturbulence $\zeta = 12 \pm 3\,\mathrm{km\,s^{-1}}$

[d] $M_{bol} = -5.05$

[e] $M_{bol} = -4.97$, calibration by North & Nicolet (1990)

[f] Macroturbulence $\zeta = 16 \pm 5\,\mathrm{km\,s^{-1}}$

[g] $v \sin i = 45\,\mathrm{km\,s^{-1}}$

[h] log g derived from photometry, $[M/H] = 0.21 \pm 0.09$, $E(B-V) = 0.068 \pm 0.010$

[j] $M_v = -3.3 \pm 0.4$, $E(b-y) = 0.025$, calibration by Napiwotzki et al. (1993)

Table 3. Times of maximum light and semi-amplitudes for the dominant mode f_1 of HN Aqr.

$T_{\max}$[HJD− 2400000.0]	Ampl. [mmag]	$N_{\rm obs}$	Band	Source of data
47008.8918(14)	21.9(13)	63	Geneva V	(1)
47397.4506(7)	16.5(4)	243	V	(2)
47791.0340(7)	15.2(4)	316	V	(3)
47801.2269(33)	26.5(30)	8	see note	(4), IUE
48144.5442(14)	11.9(7)	152	V	(3)
51445.6873(35)	29.5(49)	100	no filter	(5)NSVS
52291.0547(38)	20.7(34)	157	V	(6), ASAS-3
53301.9840(37)	20.2(30)	166	V	(6), ASAS-3
53970.8078(5)	22.1(4)	184	$B+V$	(7), mean value
56474.4318(34)	24.1(36)	90	V	(8), ASAS-SN
56900.1597(16)	22.5(16)	144	V	(8), ASAS-SN
57263.2777(15)	20.9(12)	243	V	(8), ASAS-SN
57640.5650(17)	22.7(15)	216	V	(8), ASAS-SN
57990.5867(12)	19.2(10)	263	V	(8), ASAS-SN
58066.4406(16)	21.9(16)	212	g	(8), ASAS-SN
58333.3018(13)	23.6(12)	364	g	(8), ASAS-SN
58348.5332(25)	19.8(20)	89	V	(8), ASAS-SN
58360.71848(6)	20.76(4)	9227	TESS	TESS
58375.03624(6)	20.57(5)	9088	TESS	TESS

NOTE—(1) – Waelkens & Rufener (1988), (2) – Kilkenny & van Wyk (1990), (3) – this paper, (4) – Dufton et al. (1996), IUE spectrophotometry, low-resolution, 140 – 185 nm, (5) – Woźniak et al. (2004), (6) – Pigulski & Pojmański (2008), (7) – Handler & Shobbrook (2008), (8) – Shappee et al. (2014).